The influence of alloying on the phase formation sequence of ultra-thin nickel silicide films and on the inheritance of texture

F.A. Geenen[a], E. Solano[a], J. Jordan-Sweet[b], C. Lavoie[b], C. Mocuta[c], C. Detavernier[a]

[a]*Department of Solid-State Sciences, Ghent University, 9000 Gent, Belgium*
[b]*IBM T.J. Watson Research Center, Yorktown Heights, NY, USA*
[c]*Synchrotron SOLEIL, L'Orme des Merisiers, Saint Aubin BP48, 91192 Gif-sur-Yvette, France*

Abstract

The controlled formation of silicide materials is an ongoing challenge to facilitate the electrical contact of Si-based transistors. Due to the ongoing miniaturisation of the transistor, the silicide is trending to ever-thinner thickness's. The corresponding increase in surface-to-volume ratio emphasises the importance of low-energetic interfaces. Intriguingly, the thickness reduction of nickel silicides results in an abrupt change in phase sequence.

This paper investigates the sequence of the silicides phases, and their preferential orientation with respect to the Si(001) substrate, for both 'thin' (i.e. 9 nm) and 'ultra-thin' (i.e. 3 nm) Ni films. Furthermore, as the addition of ternary elements is often considered in order to tailor the silicides' properties, additives of Al, Co and Pt are also included in this study.

Our results show that the first silicide formed is epitaxial θ-Ni_2Si , regardless of initial thickness or alloyed composition. The transformations towards subsequent silicides are changed through the additive elements, which can be understood through solubility arguments and classical nucleation theory.

The crystalline alignment of the formed silicides with the substrate significantly differs through alloying. The observed textures of sequential silicides

Email address: filip.geenen@ugent.be (F.A. Geenen)

could be linked through texture inheritance. Our study illustrates that the nucleation of a new phase drive to reduce the interfacial energy at the silicide-substrate interface as well as at the interface with the silicide which is being consumed for these sub-10nm thin films.
Keywords: nickel silicide, epitaxy, axiotaxy, texture

1. Introduction

The nickel silicides have been studied thoroughly in the past due to the beneficial properties of NiSi (e.g. low sheet resistance, low Schottky Barrier Height, low formation temperature) for usage as contact material in Si-based
5 transistor devices [1, 2, 3]. The phase formation process typically involves the annealing of an as-deposited Ni film on top of a Si substrate, resulting in the sequential formation of δ-Ni_2Si, θ-Ni_2Si, NiSi and $NiSi_2$ [4, 5, 6, 7]. Recent investigation of this '*regular*' phase sequence for relatively thick Ni films (i.e. for an as-deposited Ni thickness of e.g. 6 - 30 nm) showed that the solid-phase
10 reaction (SPR) includes a complex balance in thermodynamic parameters. For example, the phase sequence is known to include θ-Ni_2Si [5, 6, 7, 8], a transient phase which is metastable. In addition to the observation of θ-Ni_2Si, Gaudet *et al.* observes an unidentified epitaxial phase was also observed in the SPR at their lowest investigated temperature, i.e. 290 °C.

15 Due to the constant urge for miniaturisation in micro-electronic applications, the silicide contacts are trending to ever-thinner films. Surprisingly, for as-deposited and pure Ni films of only a few nanometres thick, no NiSi is formed [9, 10, 11]. It was already observed by Tung *et al.* in the early 80's that the phase sequence is significantly different when the as-deposited Ni layer is thin-
20 ner than ca. 5 nm [12, 13]. In this '*ultrathin*' SPR, the δ-Ni_2Si and NiSi phases are not formed and instead, $NiSi_2$ is already present at temperatures as low as 400 °C, at least 300 °C earlier than in the '*regular*' SPR. Intriguingly, an epitaxial, intermediate phase - with similar diffraction signature as observed in the 'regular' phase formation by Gaudet *et al.* [6] - was observed during this

ultrathin SPR, prior to the formation of low-temperature $NiSi_2$. The observation that both silicide formation regimes first form the same epitaxial phase, indicates that the origin of the shift from the regular regime to the ultra-thin regime should lie in the formation of subsequent phases. Films with these low thicknesses will receive a high energetic drive to optimise the interface alignment with the substrate. Therefore, the correlation between the silicide phase sequence and the silicides' preferential orientation is of crucial importance for these sub-10 nm thin films.

An intriguing question is how both the regular, as well as in the ultrathin film regimes, is affected through the addition of ternary elements. Indeed, silicides are often tailored through the addition of alloying elements to the as-deposited metal film, in order to alter the final properties of the formed phases [14, 15, 16, 4]. As one of the more contemporary examples, Pt-incorporation in NiSi films is known to improve the films' morphological stability, as well as to alter the preferential orientation to the Si substrate [16, 17]. Moreover, it is also reported that Pt can influence the thermodynamic stability of the intermediate silicide such as δ-Ni_2Si [18, 19, 8]. However, the influence of ternary elements on the solid-phase formation during the sequential growth of silicides in this sub-10 nm thickness region has not been studied in a systematic way. As we will show, these silicides are often epitaxially aligned with the substrate which renders them challenging to investigate by conventional, lab-based, Bragg-Brentano X-ray diffraction (XRD).

This paper investigates the phase formation in both the 'thin' (i.e. with an as-deposited Ni thickness = 9 nm) and in the 'ultrathin' (i.e. Ni thickness = 3 nm) SPR regime and how this is influenced by alloying with Pt, Co and Al. These alloying elements were selected because of their different solubility in the various nickel silicide phases. Through complementary synchrotron-based XRD measurements, we obtain a comprehensive understanding of the silicide formation, and preferential orientation of the resulting phases to the Si(001) substrate, as a function of film thickness, alloying elements and annealing temperature. This enables a discussion how the solid-phase reaction and preferential

orientation are correlated in these sub-10 nm films.

2. Experimental methods

Thin Ni films of both 3 and 9 nm thick were deposited through physical vapour deposition (PVD) on top of single crystalline Si substrates with (001) orientation. Samples for *in situ* sheet resistance measurements were sputtered on silicon-on-insulator (SOI) substrates with identical orientation and a top Si thickness of 100 nm. Prior to the deposition, these wafers received a standard chemical cleaning, following the guidelines of the Radio Corporation of America (RCA), ending with a 20 s dip in 3 % HF solution.

After reaching a base pressure of 6×10^{-7} mbar, the deposition chamber was filled with Ar up to 5×10^{-3} mbar. The deposition of Ni was performed at a relatively low sputter rate of 1.3 nm/ min, as determined through *ex situ* X-ray reflectivity (XRR) measurements. The samples were optionally alloyed with an estimated concentration of 10 at.% of Al, Co or Pt through simultaneous co-sputtering with separate sputter targets, after careful calibration of the Al, Co and Pt sputter rates on the basis of XRR. We note that the alloying species were added in *addition* to the initial Ni content. As Co and Pt are known to replace Ni atoms during silicide formation, the addition of these alloying elements render an effective increase in the metal supply to form $Ni_xM_ySi_z$ (M = Co, Pt) compounds. Other papers therefore prefer to keep the metal supply constant by reducing the Ni content when adding a ternary alloy, but such an approach is not easily translated to Al alloying, which is known to replace the Si atoms during silicide formation. For conciseness, these samples will be referred to as Ni(Al), Ni(Co) and Ni(Pt).

The samples were then annealed in a dedicated *in situ* X-ray diffraction (XRD) set-up at the X20C-beamline of the NSLS synchrotron (Brookhaven, USA). The synchrotron provides adequate X-ray brightness to investigate these ultra-thin samples. The solid-phase reaction between the film and the substrate was monitored during an anneal at a rate of 1 °C/ sec in a He(5 %H_2) ambient,

as these samples are otherwise prone to oxidation during the annealing process. The X-rays, with a wavelength of $\lambda = 0.180\,\mathrm{nm}$ (i.e. an energy of $6.88\,\mathrm{keV}$) diffract on the sample in a fixed geometry, therefore only monitoring diffraction signal originating from planes nearly-parallel to the sample's surface. The diffracted intensities were monitored using a custom-build linear detector with a total angular acceptance of 14° in 2θ. These diffractograms are plotted as a function of temperature and diffraction angle using a grayscale map for the recorded intensity values, where black indicates the highest intensity. A similar annealing set-up was used for *in situ* sheet resistance measurements during temperature treatment through a four-point probe approach with identical annealing conditions. The measured resistance of the samples were at least one order of magnitude lower compared than the *in situ* resistance of bare SOI substrates at each temperature. The set-up does not guarantee an identical probe geometry between separate measurements, and as such the measured resistances will be plotted on a relative scale, instead of an absolute scale, as a function of temperature.

As-deposited samples were alternatively quenched from specific temperatures for *ex situ* pole-figure measurements for crystal phase identification and characterisation of the preferential orientation, also known as crystalline texture. A total of 100 samples were measured in order to obtain a quasi-continuous dataset as a function of quench temperature. These *ex situ* measurements were performed at the DiffAbs beamline of the SOLEIL synchrotron (Gif-sur-Yvette, France) [20]. The incidence X-ray beam is monochromatized using a double-crystal monochromator to a wavelength of $\lambda = 1.55\,\mathrm{nm}$ (i.e. an energy of $8\,\mathrm{keV}$). A 6-circles diffractometer in kappa geometry was used together with a hybrid pixel area detector (XPAD detector of 240×560 pixels, with a pixel size of 130 by 130 µm) [21, 22, 23, 24]. The long side of the detector was mounted in the 2θ direction, resulting in an angular acceptance determined to be 32°, and around 13° in the perpendicular direction. The area detector acquired a snapshot every 100 ms during a continuous in-plane rotation of the samples' azimuth (denoted as the ϕ angle), rotating at a speed of $8\,^{\circ}\,\mathrm{s}^{-1}$ and covering 110° in ϕ.

The sample was then rotated in the elevation angle χ in steps of 5° from 0 to 85°, rendering significant overlap between two sequential χ steps. This set-up enables the measurement of a set of pole figures within 4.5 min. Every sample was measured at least three times without re-aligning the sample, in order to
120 obtain adequate diffraction statistics for these sub-10 nm thin films.

The raw data were re-calculated to angular (χ, ϕ and 2θ) space and the resulting datasets are presented in this paper in polar coordinates with an equal-area projection and a logarithmic-intensity gray-scale with black indicating the highest intensities. The acquired data were symmetrized to a full 360° ϕ cov-
125 erage, exploiting the four-fold symmetry of the Si(001) substrate. These pole figures were analysed using a home-developed software package, GUSTAV [25], in order to determine the preferential orientations of the silicides.

3. Results

We report on the SPR between the (un)alloyed Ni films with the Si substrate
130 for two different Ni thicknesses: 3 and 9 nm. As mentioned in the previous paragraph, *in situ* XRD measurements allow continuous phase identification as a function of temperature, on the condition that the diffracting planes are oriented (nearly) parallel to the sample's surface. Epitaxial phases, which do not necessarily fulfil this condition, are alternatively observed through the *ex situ*
135 pole figures. The latter measurements will also be used to assess the preferential orientation of the silicide grains with respect to the Si(001) substrate. These orientations will be expressed in terms of lattice planes, and table 1 provides an overview of the unit cells of the occurring nickel silicide phases.

9 nm *Ni films*

140 The *in situ* XRD measurement of an unalloyed, 9 nm Ni film is displayed in figure 1a. The SPR shows the transformation of the initial Ni diffraction peak at room temperature, into the δ-Ni_2Si around 230 °C by the observation of the δ-Ni_2Si (301) plane at $2\theta = 53.6°$. The peak at $2\theta = 56.4°$, observed in a small

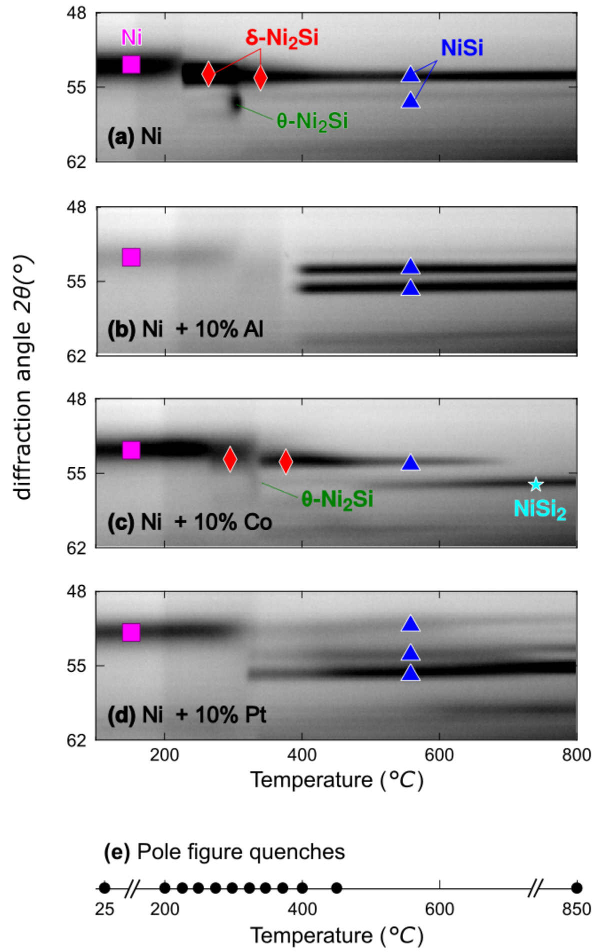

Figure 1: *In situ* XRD measurements of 9 nm thick Ni films: unalloyed **(a)**, and alloyed with 10 at.% Al **(b)**, Co **(c)** and Pt **(d)**. These measurements allow to determine the important temperature regions where quenches were made for further *ex situ* investigation **(e)**, in addition to a measurement at room temperature.

Table 1: Overview of the binary nickel-based phases observed in this paper.

Phase	*Lattice*	a (Å)	b (Å)	c (Å)	*JCPDS No.*
Ni	FCC	3.524	-	-	00-004-0850
δ-Ni_2Si	Orth.	7.066	5.008	3.732	00-048-1339
θ-Ni_2Si	Hex.	3.805	-	4.890	01-073-2093
NiSi	Orth.	5.233	3.258	5.659	00-038-0844
$NiSi_2$	FCC	5.406	-	-	03-065-2974

temperature window of ca. 20 °C around 300 °C was discussed in a study by Gaudet *et al.* [6], and is related to a fiber-textured θ-Ni_2Si . This θ-Ni_2Si phase is then consumed, after which δ-Ni_2Si and NiSi are present. Around 450 °C, δ-Ni_2Si is also consumed leaving NiSi as the only observed phase during the rest of the *in situ* annealing experiment.

Similar measurements on Ni samples which are alloyed with 10 at.% Al, Co and Pt (Fig. 1 b,c and d) show clear differences with the above observations. (i) The as-deposited Ni(Al) layer diffracts with much lower intensity, which can be explained by a lower crystalline-order of the as-deposited layer due to the incorporation of Al in the Ni lattice through the co-sputtering of both materials. However, the Ni-diffraction peak at $2\theta = 53.0°$ is still observable and is consumed around 300 °C. No clear silicide phase can be identified immediately thereafter. Instead, a broad background is observed, which diminishes for a small temperature window of 20 °C just prior to the formation of NiSi. The latter phase is then the only phase remaining throughout the annealing experiment. Comparing the relative diffracted intensities of the NiSi (112) peak ($2\theta = 54.0°$) to the (202/211) peak ($2\theta = 55.8°$) already hints that the texture of this phase is different from the NiSi texture formed from the pure Ni film. No intermediate phases such as δ-Ni_2Si or θ-Ni_2Si are observed via *in situ* XRD during the annealing process. (ii) The annealing of a Ni(Co) layer is comparable to the pure Ni reference measurement up to 500 °C, with the similar observation of δ-Ni_2Si and θ-Ni_2Si. At higher temperatures, the formation of $NiSi_2$ is observed as seen through the occurrence of its diffraction peak at $2\theta = 56.0°$ and 33.5° (the latter

visible through measurements at a different 2θ diffraction window), far earlier than for unalloyed Ni, where it would only form above 850 °C. (iii) Finally, the *in situ* XRD of Ni(Pt) does not contain clear diffraction of intermediate
170 Ni_2Si phases. Furthermore, similar to the Ni(Al) sample, there is a significant difference in observed intensity of the NiSi peaks, where now the most intense peak is originating from the (202)/(211) planes ($2\theta = 55.8°$), again indicating a significant change in preferential orientation.

The *in situ* XRD measurements indicate that most of the formed phases are
175 observed between 200 and 400 °C. Therefore, *ex situ* pole figures are measured for samples quenched every 25 °C in this temperature window, in addition to an as-deposited sample, and quenched samples at 450 and 850 °C (Fig. 1e). For each of these 48 samples, sets of *ex situ* pole figures were acquired using an area detector, resulting in one pole figure for every value of 2θ in between 30 and 62°
180 in a quasi-continuous fashion, due to the 540 pixels along the 2θ direction. A selection of the measured pole-figure data is shown in figure 2, which contains the integrated diffracted intensities around $2\theta = 45.5° \pm 0.4°$ (d = 1.98-2.01 Å, corresponding to $2\theta = 53.6° \pm 0.5°$ for the X-ray wavelength used during the *in situ* XRD measurements). This broad 2θ window includes diffraction intensities
185 from the Ni(111), δ-Ni_2Si(301/121), θ-Ni_2Si(102/110) and NiSi(112) planes and serves as an overall illustration of all observed phases. Si(220) diffraction is also measured, and the position of these epitaxial spots are indicated on the pole figures (e.g. Fig. 2b-i). Other pole figures from the complete set of pole figures (of which a selection will be discussed further) were used to corroborate the
190 phase identification and their texture during the analysis.

In the following overview of our results concerning the 9 nm Ni films, we first discuss the texture of every occurring phase, as observed for the four differently-alloyed samples. Thereafter, the change in diffracted intensities of those phases is addressed as a function of temperature, which allows to interpret the rate
195 of formation and consumption of these phases and compare these with *in situ* XRD measurements.

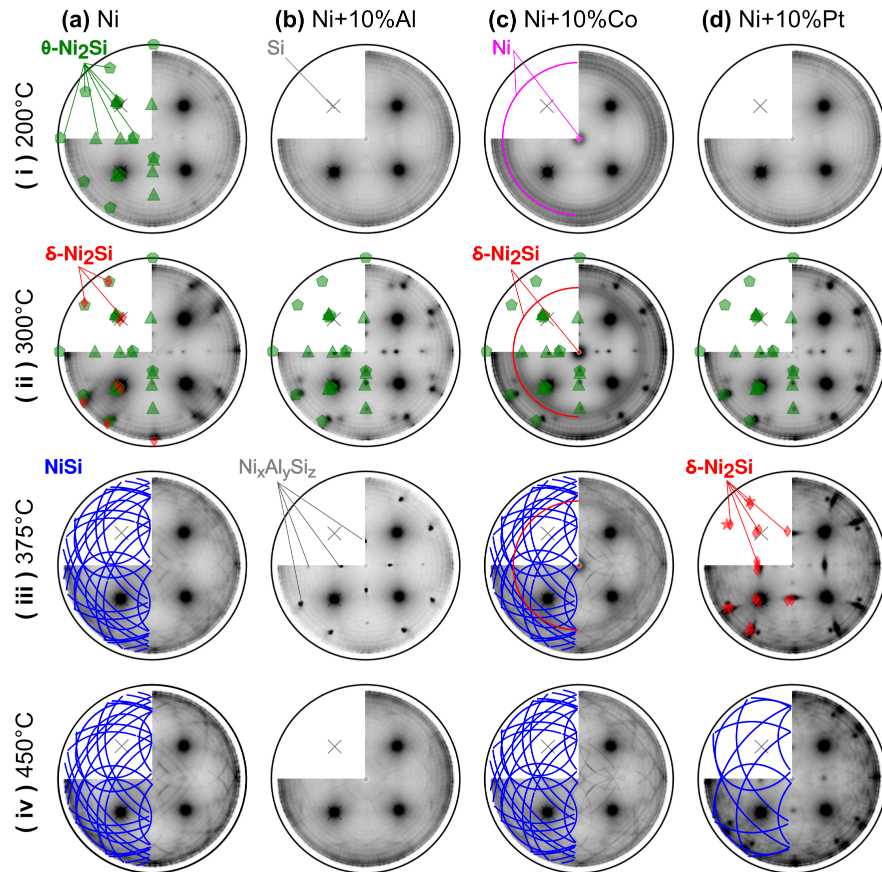

Figure 2: A selection of the aquired pole-figure dataset for alloyed and unalloyed 9 nm Ni films, displaying the integrated diffraction intensities around $2\theta = 45.5° \pm 0.4°$. These images examplify the observed phases and their textures. The identified silicide textures are overlapped on the left half of the dataset (using the symbols defined in tables 2, 3 and 4). The Si(220) diffraction peak is always visable and indicated with a gray cross.

Table 2: Overview of observed epitaxial orientations of the θ-Ni_2Si phase for all 3 and 9 nm films (symbols used in figures 2 and 8). The angular mismatch between the film and substrate, as calculated from the proposed alignments, are given in terms of $\Delta\chi$ and $\Delta\phi$.

Symbol	*Plane alignments*	$\Delta\chi$ (°)	$\Delta\phi$ (°)
A_θ (⬟)	$(02\bar{2}1)_\theta \sim //(\bar{2}22)_{Si}$	0.2	0.0
	$(\bar{2}110)_\theta \sim //(220)_{Si}$	0.1	0.1
	$(000\bar{1})_\theta \sim //(1\bar{1}1)_{Si}$	0.6	0.8
B_θ (▲)	$(02\bar{2}1)_\theta \sim //(222)_{Si}$	0.2	0
	$(\bar{2}110)_\theta \sim //(\bar{2}20)_{Si}$	0.1	0.1
	$(0001)_\theta \sim //(\bar{1}\bar{1}5)_{Si}$	0.16	0.85

Overview of observed textures. The pole figures of unannealed samples (not shown) indicate that the crystalline grains of Ni, Ni(Al) and Ni(Pt) do not have a strong preferential orientation, and as such, the pole figures do not
200 show significant changes in intensity as a function of χ or ϕ. Ni(Co), on the other hand, exhibits higher diffraction signal at the center of the pole figure (comparable to Fig. 2c-i) and a diffraction ring near $\chi = 70°$. The concentric diffraction ring is typically observed for a fiber texture, for which a specific crystalline direction acts as a rotation axis perpendicular to the sample's surface.
205 The higher diffraction at the center of the pole figure indicates that the Ni-lattice (111) plane is oriented perpendicular to this center of rotation, which coincides with a diffraction ring at $\chi = 70.5°$ due to the cubic symmetry of the Ni unit cell (e.g. the angle between Ni(111) and Ni(11$\bar{1}$)), and also explains the diffraction ring of the Ni(200) plane (not shown) at $\chi = 54°$.

210 Annealing these samples up to 200 °C provides a slight increase of small diffraction spots (figure 2 a-i), indicating the presence of an epitaxial phase. The same diffraction pattern is observed for all samples annealed at 300 °C, and is identical to the epitaxial phase observed for 3 nm films at 350 °C [9, 26] which was identified as an epitaxial θ-Ni_2Si. The observed diffraction spots of θ-Ni_2Si
215 can be explained by two different epitaxial alignments with the Si substrate (Table 2, where A_θ has the highest observed diffracted intensity) [27, 26], whose positions are overlaid by green circles in figures 2ii. The approximate alignment

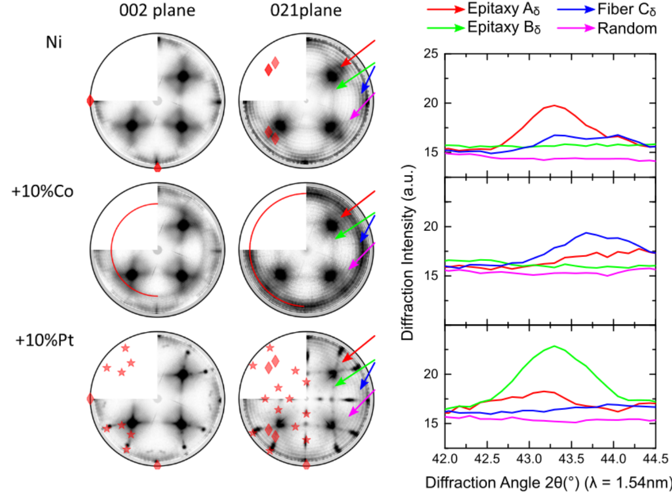

Figure 3: **Left:** The pole figures which contain diffraction of δ-Ni_2Si show that both epitaxial (Ni, Ni(Pt)) and fiber-aligned (Ni, Ni(Co) silicide are present, depending on the composition of the initial 9 nm Ni film. The red, green and blue arrows indicate positions which are uniquely correlated with a specific texture type. The pink arrow is choosen as such that none of the observed textures should diffract here. **Right:** The diffraction at these positions is plotted as a function of 2θ for the (021) plane. Note that no δ-Ni_2Si diffraction is observed at orientations corresponding with randomly-aligned grains.

for the {0001} planes are also given to initiate further discussion. It is interesting to note that we observed no diffraction signal originating from θ-Ni_2Si that is
220 aligned in a random distribution with the substrate, which explains their absence in the conducted *in situ* XRD measurements.

The δ-Ni_2Si phase can be observed for Ni, Ni(Co) and Ni(Pt) in figures 2a-ii, c-ii and d-iii films but did not occur for any quenched Ni(Al) sample. Remarkably, the texture of the δ-Ni_2Si is significantly affected by alloying the
225 Ni film. Additional pole figures of the δ-Ni_2Si(002) and (021) planes are shown in figure 3. Two different texture types are observed: epitaxial alignment for unalloyed Ni and Ni(Pt), and fiber-aligned δ-Ni_2Si for Ni(Co). For unalloyed Ni, the preferential orientation can be mostly described as an epitaxial alignment, in addition to a low-intense fiber alignment. No diffraction is observed
230 from randomly-oriented grains, as indicated in the right side of figure 3. The

Table 3: Overview of observed epitaxial (A_δ, B_δ) and fiber (C_δ) orientation of the δ-Ni_2Si phase as observed for 9 nm Ni, Ni(Co) and Ni(Pt) films (symbols used in figures 2 and 3). The angular mismatch between the film and substrate, as calculated from the proposed alignments, are given in terms of $\Delta\chi$ and $\Delta\phi$.

Symbol	*Plane alignments*	$\Delta\chi$ (°)	$\Delta\phi$ (°)	*occurrence*
A_δ (♦)	$(001)_\delta \sim //(110)_{Si}$	0	0	Ni, Ni(Pt)
	$(301)_\delta \sim //(20\bar{2})_{Si}$	1.9	0.8	
	$(0\bar{1}0)_\delta \sim //(1\bar{1}1)_{Si}$	0	0.4	
B_δ (★)	$(001)_\delta \sim //(110)_{Si}$	0	0	Ni(Pt)
	$(121)_\delta \sim //(20\bar{2})_{Si}$	2.7	1.4	
	$(010)_\delta \sim //(\bar{1}\bar{1}5)_{Si}$	0.2	0.4	
C_δ (–)	$(301)_\delta \sim //(00\bar{2})_{Si}$	0.0	0.0	Ni(Co)

identification of the epitaxial alignments observed within the Ni and Ni(Pt) samples is given in table 3. The fiber-texture, which was more clearly observed in the Ni(Co) sample, was determined to be originating from a $(301)_\delta//(002)_{Si}$ alignment. Gaudet *et al.* also observed this fiber alignment of δ-Ni_2Si for an-
235 nealed, unalloyed, Ni films of 30 nm thickness [28]. The origin of the observed diffraction peak during the *in situ* XRD measurements (Fig. 1) is explained by grains that are oriented along the fiber-alignment, as the set-up was detecting planes which were parallel to the substrate's surface (i.e. Si{001}).

For Ni(Al), an epitaxial phase is observed at 375 °C (labelled as $Ni_xAl_ySi_z$
240 in Fig. 2b-iii), in agreement with the phase observed in a recent study on the Ni(Al) silicide formation process for thicker Ni films [29]. Its occurrence is indicated by additional diffraction peaks at $2\theta = 22.4$, 24.9, 32.1, 36.7 and 38.6°, but no match could be found with reference diffraction patterns in the JCPDS database, preventing a clear phase identification. The ternary Ni-Al-Si
245 phase diagram [30, 31, 32] does include several ternary phases, and not all of the crystal structures are available in the literature.

At higher temperatures, the NiSi phase is present within all of the samples. Pole figures for this NiSi phase (Fig 2) exhibit a complex pattern of circular features, which is indicative for the axiotaxial texture previously discussed by

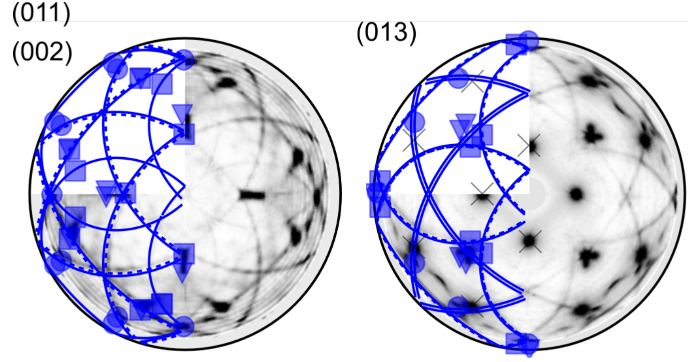

Figure 4: The 9 nm Ni(Pt) pole figures which display diffraction of NiSi contain both axiotaxial (circular lines) as well as epitaxial (local spots of higher intensity) features. The overlayed epitaxies are listed in table 4.

Table 4: Overview of observed epitaxial orientation of the NiSi phase (symbols used in Fig. 4). The angular mismatch between the film and substrate, as calculated from the proposed alignments, are given in terms of $\Delta\chi$ and $\Delta\phi$.

Symbol	*Plane alignments*	$\Delta\chi$ (°)	$\Delta\phi$ (°)	*occurrence*
A_{NiSi} (■)	$(\bar{1}0\bar{1})_{NiSi} \sim //(101)_{Si}$	0	0	Ni(Pt), 9 & 3 nm
	$(300)_{NiSi} \sim //(2\bar{2}\bar{2})_{Si}$	3.7	2.9	
	$(010)_{NiSi} \sim //(10\bar{1})_{Si}$	0	0	
B_{NiSi} (▼)	$(21\bar{1})_{NiSi} \sim //(\bar{2}20)_{Si}$	0	0.96	Ni(Pt) 9 nm
	$(013)_{NiSi} \sim //(1\bar{1}0)_{Si}$	0	0	
	$(100)_{NiSi} \sim //(111)_{Si}$	4.78	0	
C_{NiSi} (●)	$(211)_{NiSi} \sim //(02\bar{2})_{Si}$	1.36	3.93	Ni(Pt), 9 nm
	$(013)_{NiSi} \sim //(\bar{1}10)_{Si}$	3.13	0.1	
	$(100)_{NiSi} \sim //(\bar{1}\bar{1}\bar{5})_{Si}$	0.0	4.1	

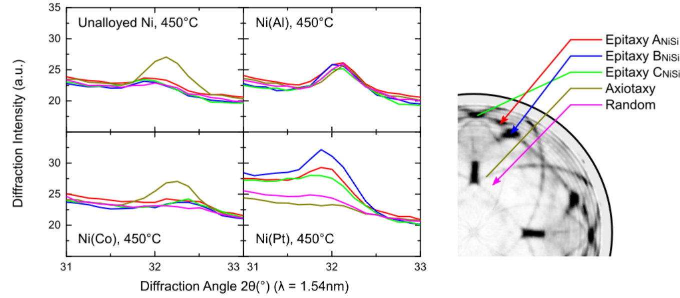

Figure 5: (*color version online*)The XRD intensity is displayed as a function of 2θ for different regions in the reciprocal space, which are selected to represent the different textures observed for NiSi.

250 Detavernier *et al.* [33]. The axiotaxy originates from the preferential alignment of lattice planes with a similar d-spacing across the interface. Two axiotaxial axes are observed here: $(202)_{NiSi}//(202)_{Si}$ and $(211)_{NiSi}//(202)_{Si}$, in agreement with our earlier work [33]. The patterns for the unalloyed Ni sample are almost identical to the patterns observed from a Ni(Co) sample (Fig. 2a,b-iii,iv).
255 The intensity of these circular features is, however, significantly reduced for the Ni(Al) sample, where the NiSi phase diffracts more uniformly for every χ and ϕ value, indicating a more random distribution of the grains' orientations (Fig. 2b-iv). NiSi formed from the Ni(Pt) sample also contains local diffraction spots of higher intensity along the circular features, indicating that the rotational
260 freedom, which is allowed along the axiotaxial rotation axis, is reduced with a second alignment condition, thus pinning these grains in an epitaxial alignment (Fig. 2d-iv). The fitted epitaxial components are displayed in figure 4 and listed in Table 4.

Figure 5 allows a more quantitative comparison between the different tex-
265 tures of the NiSi phase. For unalloyed Ni (and Ni(Co)), it is clear that the diffraction along the axiotaxial line has the highest intensity, whereas the regions associated with epitaxial alignment do not diffract more than a region which is corresponding to a randomly-oriented grain. As such, there is no preference for the grains to align themselves along this epitaxial texture. A similar

270 plot for the Ni(Al) sample clearly shows the absence of any specific preferential orientation for the latter alloy: diffraction is more or less uniform for every direction. For Ni(Pt), we observe that the regions associated with the different epitaxial orientations have significant higher intensity than a randomly-chosen orientation, thus confirming the preferential alignment

275 *Evolution of textured diffraction as a function of temperature.* From every observed phase in the *ex situ* pole-figure measurements, a specific region within χ, ϕ and 2θ was selected that was isolated from the diffraction of other phases, and the diffraction intensity was subsequently fitted after a local background subtraction. The evolution of the fitted intensities as a function of tempera-
280 ture is displayed in figure 6. In order to depict the evolution of the different phases as a function of temperature, we have plotted the relative intensity, i.e. normalized to the maximum observed intensity of that particular phase while differentiating for the four different as-deposited compositions. This provides an overview of the phase sequence similar to the *in situ* XRD technique, but
285 the pole figures allowed to include textured phases such as epitaxial θ-Ni_2Si. The arrows between different phases will be further explained in the discussion section.

In the *in situ* XRD measurements, a small temperature window exists for the Ni and Ni(Co) sample where diffraction was observed at $2\theta = 56.4^{\circ}$, related to a
290 fiber-textured θ-Ni_2Si [6], which is not observed within the pole-figure measurements. We relate this inconsistency to either an instability of this phase during quenching, or that this particular phase's temperature window is slightly smaller than the temperature difference between two *ex situ* pole-figure quenches.

3nm Ni films

295 For Ni films of 3 nm as-deposited thickness, a slightly different approach was needed, as the *in situ* XRD diffraction of the Ni, Ni(Al) and Ni(Co) samples did not contain any distinguishable change in diffraction signal, and thus doesn't provide any information on the SPR, similar to the results of De Keyser *et*

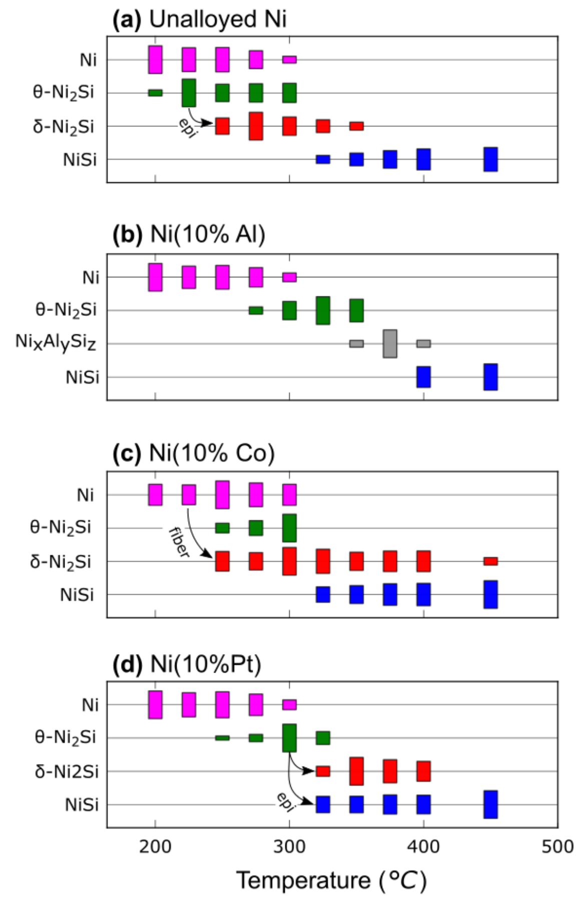

Figure 6: Overview of the observed silicides' diffraction intensity as a function of temperature for pure and alloyed 9 nm Ni films. The observed intensities are proportional to the height and normalised to the maximum occuring intensity per sample. Arrows indicate examples of texture inheritance across multiple phases, as explained in the discussion.

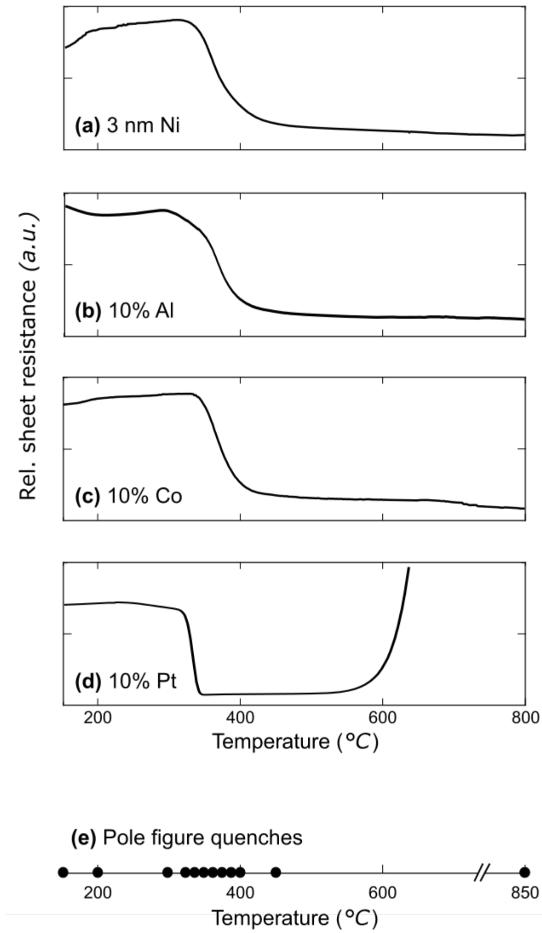

Figure 7: Relative evolution of the sheet resistance of 3 nm Ni films with variable as-deposited composition, as measured through *in situ* sheet resistance measurements on SOI substrates. The bottom panel **(e)** shows the quenching temperatures of the samples prepared for *ex situ* pole-figure measurements, in addition to a room-temperature sample.

al. [9]. Alternatively, *in situ* sheet resistance measurements can be used to monitor transitions of the formed silicides during the annealing. Indeed, as shown in figure 7a, the sheet resistance of an unalloyed Ni film shows relatively high resistance between 150 and 300 °C, followed by a decrease between 300 and 400 °C. Thereafter, the resistance decreases at slower pace further up to 850 °C. Similar behaviour is observed for Ni(Al) and Ni(Co). The sheet resistance in Ni(Pt) also contains a decrease in sheet resistance around 340 °C, within a narrower temperature window. However, the low-resistive state is only stable up to 600 °C, after which the resistance dramatically increases, which is typically observed when NiSi is agglomerating [34, 4, 9].

The *in situ* sheet resistance measurements allow to determine that a significant change in the sample structure is occurring between 300 and 400 °C. Therefore, quenches were made for *ex situ* pole-figure investigation every 12.5 °C between 325 and 400 °C, in addition to an as-deposited film and samples quenched at 150, 200, 300, 450 and 850 °C (Fig. 7e). A selection of the acquired pole-figure datasets is displayed in figure 8.

The absence of diffraction intensity from an as-deposited layer can be understood, as it is known that the sputter deposition process of the first Ni monolayers form an amorphous, intermixed, Ni(Si) layer [9, 35]. It is suggested that this amorphous layer contains an inherent concentration gradient, which could promote the formation of θ-Ni_2Si as this phase can locally adapt its composition within a range of 33 up to 42 at % Si [36, 37]. For these ultrathin films, the formation of NiSi is only observed for the Ni(Pt) sample, coinciding with the consumption of θ-Ni_2Si around 325 °C. Similar to the 9 nm Ni(Pt) film, NiSi forms with clear epitaxial features along epitaxial rings (Table 4). For the 3 nm Ni, Ni(Al) and Ni(Co) as-deposited samples, epitaxial θ-Ni_2Si is also present, but no silicide phase appears while θ-Ni_2Si is consumed. No other phases, such as as-deposited Ni, δ-Ni_2Si or $NiSi_2$, could be observed in any of the quenched 3 nm samples.

We can assume that the slow consumption of θ-Ni_2Si for Ni, Ni(Al) and Ni(Co) is associated with the formation of epitaxial $NiSi_2$, based on the liter-

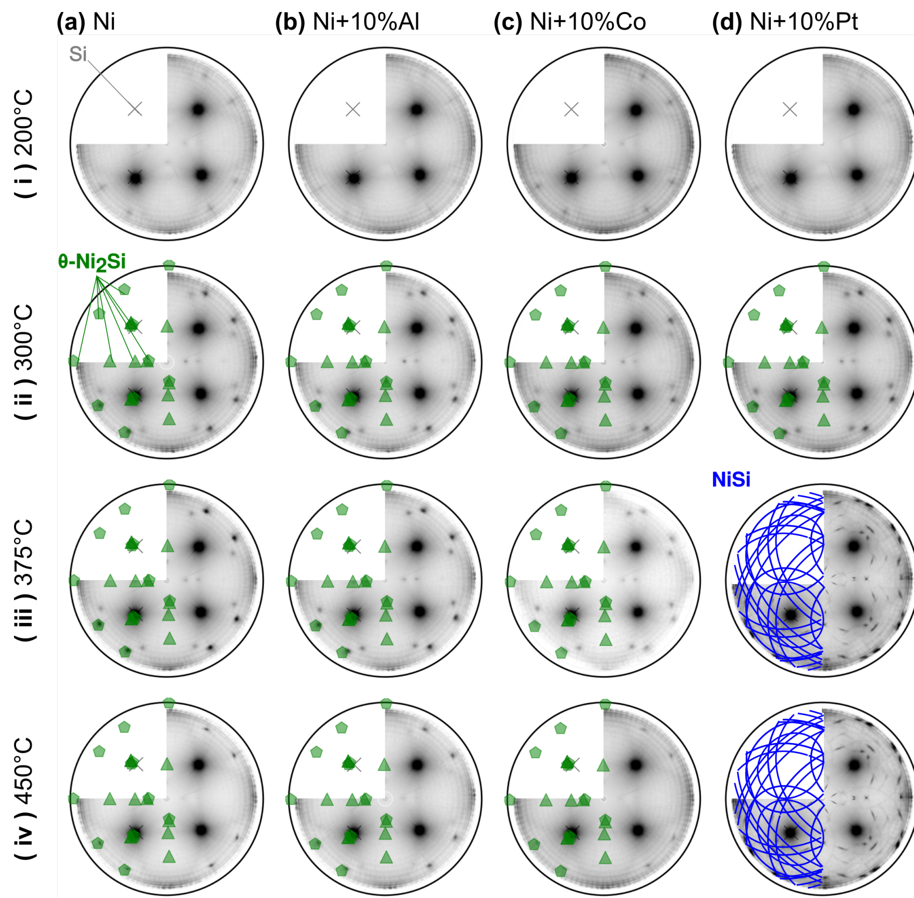

Figure 8: A selection of the aquired pole-figure dataset for alloyed and unalloyed 3 nm Ni films, displaying the integrated diffraction intensities $2\theta = 45.5^{\circ} \pm 0.4^{\circ}$. These images examplify the observed phases and their textures. The identified silicide textures are overlapped on the left half of the dataset (using the symbols defined in tables 2 and 4). The Si(220) diffraction peak is always visable and indicated with a gray cross.

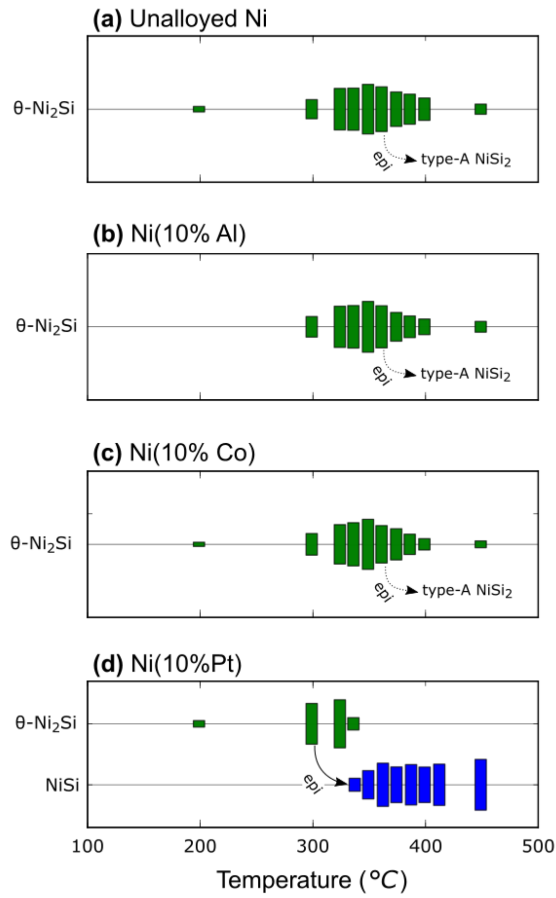

Figure 9: Overview of the observed silicides' diffraction intensity as a function of temperature for pure and alloyed 3 nm Ni films. The observed intensities are proportional to the height and normalised to the maximum occuring intensity per sample. Arrows indicate examples of texture inheritance across multiple phases, as explained in the discussion.

ature [12, 13, 38, 9, 26, 10, 11]. This is corroborated by the slow decrease of the *in situ* sheet resistance measurements: as $NiSi_2$ exhibits a lower resistance due to an increase in layer thickness and an assumed lower bulk-resistivity than θ-Ni_2Si. Due to the very similar crystal structure of $NiSi_2$ and the Si substrate (with only 0.46% difference in lattice parameter), the diffraction angles 2θ are almost identical. Moreover, it is known that the $NiSi_2$ phase can grow in an identical alignment with the Si substrate for such thin initial Ni films, i.e. $(100)_{NiSi2}//(100)_{Si}$ and $(001)_{NiSi2}//(001)_{Si}$ (also known as the type-A epitaxial alignment of $NiSi_2$). This particular orientation is not observable from our *ex situ* pole-figure measurements, as the recorded scattered intensity is highly dominated by the vicinity of the Si substrate Bragg peaks. However, TEM-based studies in the literature observed the type-A epitaxial alignment of $NiSi_2$ [12, 26, 10].

The formation and consumption of the observed phases is illustrated in figure 9. It is clear that the epitaxial θ-Ni_2Si slowly is consumed at the same temperatures at which the signal within *in situ* sheet resistance measurements decreases.

4. Discussion

Our *in situ* XRD and *ex situ* pole-figure measurements clearly indicate that alloying not only influences the temperature windows in which specific silicide phases occur, but also can change the phase sequence (e.g. through the formation of NiSi in the ultrathin thickness regime with Pt alloying) as well as the preferential orientation of the occurring phases. We first discuss the observed change in phase sequence and temperature window in the context of alloy solubility. Thereafter, we discuss and rationalise the observed preferential orientations.

Influence of alloying on phase formation

The temperature windows of the presence of δ-Ni_2Si, θ-Ni_2Si, and NiSi are significantly influenced through alloying for 9 nm Ni films, as depicted in figures

Table 5: The maximum atomic concentrations of Al, Co and Pt ternary elements in nickel silicides. * indicates that a full replacement of Ni is possible. Arrows indicate an observed increased (↗) or decreased (↘) width of the temperature window of the phase presence, according to *ex situ* pole-figure and *in situ* XRD measurements (Fig. 1, 6)

Alloy:	Al (%)		Co (%)		Pt (%)	
δ-Ni_2Si	20	–	66*	↗	< 5	↘
θ-Ni_2Si	20	↗	unknown	↘	soluble	–
NiSi	1.5	↘	10	↘	50*	↗
$NiSi_2$	29	–	33*	↗	< 5	–
Ref.	[30, 31, 32]		[39]		[40, 36, 18, 41]	

1 and 6. For example, we observe that the formation of δ-Ni_2Si is delayed when Pt is present as alloying element, whereas Co, on the other hand, seems to stabilise the δ-Ni_2Si phase up to higher temperatures. We correlate these changes in the observed temperature windows with the solubility of the alloying element in the silicide phase (the maximum atomic concentration that can be in solid-solution within the silicide compounds are tabulated in Table 5) together with the observed changes of the phases' existence temperature windows. This effect can be understood within the framework of classical nucleation theory [42], where the energetic barrier for a phase to nucleate is related to the change in enthalpy of formation, the change in entropy and the change in interfacial energy upon phase transition. The enthalpy of formation of these nickel silicides are comparable: $\delta - Ni_2Si$: -46.9, $NiSi$: -42.4, $NiSi_2$: 29.3 kJ/mol of atoms [43]. However, the nucleation barrier to form these phases will be influenced through alloying. An alloy with low solubility in a particular silicide phase will indeed hinder the formation of this new phase, as the alloying element should first be expelled before the new crystal structure can nucleate. This effect has in fact been observed by Mangelinck *et al.* through atom probe tomography, as Pt is segregated to the grain boundaries of δ-Ni_2Si, also known as the snowplough effect [18, 19]. On the other hand, a soluble alloy will enable an increase in entropy within a silicide grain, and as such, potentially lower the nucleation energy barrier to form this new phase. Through this argument,

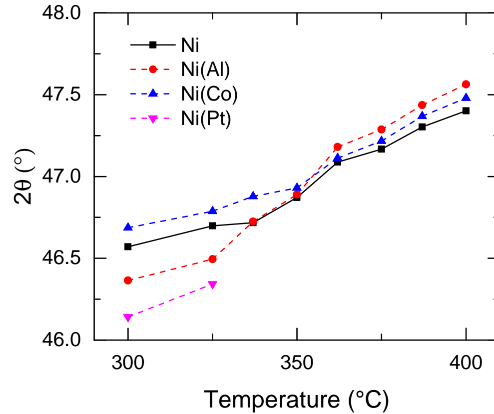

Figure 10: (color online) Evolution of the 2θ position of an epitaxial peak of the θ-Ni_2Si (near $\chi = 18^\circ$ and $\phi = 0^\circ$) as observed in 3 nm Ni films.

380 we can understand several aspects of the observed phase sequence for the 9 nm films, including the larger temperature window of δ-Ni_2Si with Co-alloying, how the same alloy promotes the low-temperature $NiSi_2$ formation, and the delay in NiSi formation through Al alloying. The solubility argument is, of course, not the only condition for changes in the temperature window (e.g. the absence
385 of δ-Ni_2Si when Al alloying is used). Other thermodynamic parameters, such as interfacial energy through substrate alignment and change in diffusion rates at grain boundaries will also contribute to the observed shifts in temperature windows. This will be discussed further below.

For 3 nm Ni layers, it is remarkable that the formation of the epitaxial θ-
390 Ni_2Si does not seem to be influenced by Al or Co alloys. Indeed, θ-Ni_2Si has similar growth profiles and diffraction intensities for Ni, Ni(Al) and Ni(Co) samples at this thickness, and its formation does not seem to be hindered by the alloying element. One may argue that the lattice of θ-Ni_2Si, which can cover from 33 to 42 %Si according to the binary Ni-Si phase diagram [36], can eas-
395 ily adapt to the incorporation ternary atoms. This would imply a significant strain in the lattice, and by consequence a shift in the diffraction angle of θ-Ni_2Si. To verify this, we fitted the 2θ peak positions of the θ-Ni_2Si epitaxial

peak at $\chi = 18^{\circ}$, which has a high diffraction intensity and its low elevation angle χ ensures a decent resolution in 2θ (Fig. 10). Two significant changes
400 can be observed. (i) As function of temperature, the diffraction angle increases linearly, corresponding to a decrease in lattice parameters from 1.95 to 1.92 Å over a 100 °C temperature range. This decrease can be related to a change in film strain, composition or due to a negative coefficient of thermal expansion of at least one lattice parameter. The reduction of the crystalline lattice is sig-
405 nificantly higher when compared to other silicides with a negative coefficient of thermal expansion [44]. Unfortunately, too little diffraction planes with sufficient intensity were observed in these measurements to further investigate this effect. (ii) As function of alloying species, one can observe that the diffraction peak is systematically higher in 2θ when Co alloying is used in comparison with
410 an unalloyed sample, which is similar to the effect of Co-alloying on the NiSi or $NiSi_2$ phase [45]. Al and Pt seem to increase the initial θ-Ni_2Si lattice spacing (corresponding to a lower 2θ angle), and the subsequent evolution of the Ni(Al) sample indicates a complex change in the films' composition or strain. This illustrates the flexibility of the θ-Ni_2Si to accommodate alloying elements and
415 compositional gradients, which possibly explains why no significant change can be observed in the growth profile within the ultrathin film region. This is again corroborated through the texture of θ-Ni_2Si: although the texture of other silicides changes remarkably with the addition of a ternary element (Figures 3 4), the same epitaxy is always observed for θ-Ni_2Si, independent of as-deposited
420 composition or thickness (Figures 2 8).

Influence of alloying on preferential orientation - examples of texture inheritance

Not only the temperature windows of the observed phases is influenced through alloying, but also the silicides' preferential orientation with respect to the Si substrate. The most remarkable changes can be found in the texture
425 of δ-Ni_2Si, where an epitaxial orientation is observed for Ni and Ni(Pt) and a fiber texture for Ni(Co) (Fig. 3 and Table 3)). Moreover, the overview of pole-figure measurements (Fig. 2) illustrates that the fiber texture is most clearly

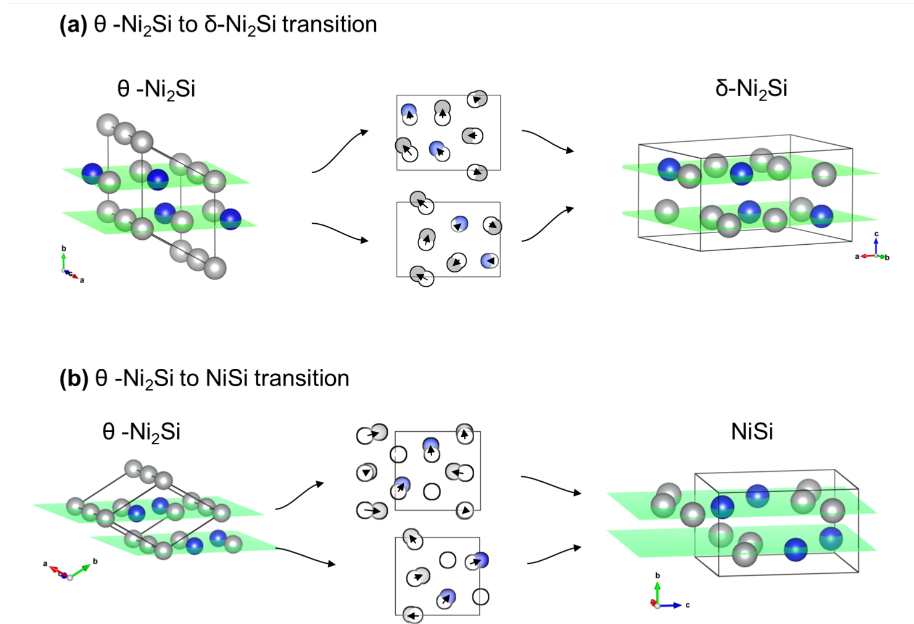

Figure 11: The transition from **(a)** θ-Ni_2Si to δ-Ni_2Si or from **(b)** θ-Ni_2Si to NiSi involves only minimal atomic movement, thus possibly introducing texture inheritence.

present in the as-deposited cobalt-alloyed nickel layer, as well as in subsequent δ-Ni_2Si. This could indicate that the texture of a specific silicide is influenced
430 by the orientation of the preceding phase. Indeed, Gaudet *et al.* [6] reported, for the unalloyed nickel silicide solid-phase reaction, that a transformation from one phase to another phase could coincide in an inheritance of fiber-textures, provided that the crystal structures are similar. A similar reasoning applied here for a fiber-inheritance between the as-deposited, cobalt-alloyed Ni(111)
435 fiber-axis and δ-Ni_2Si (301), where the respective fiber planes evolve from a d-spacing of 2.03 to 1.99 Å, allowing plane-to-plane matching at the nucleation interface between cobalt-alloyed nickel grains and δ-Ni_2Si.

A more remarkable texture inheritance is indicated by our measurements on some of the observed *epitaxial* orientations. We explain this phenomenon on the
440 basis of the epitaxially textured δ-Ni_2Si when Pt is added as a ternary element. The epitaxial alignment of δ-Ni_2Si , which is not present when δ-Ni_2Si is formed

from an unalloyed Ni film (Fig. 3), would be hard to explain on solubility arguments alone, as the solubility of Pt in δ-Ni_2Si is very low. However, this phase is formed at expense of the preceding, epitaxially-aligned, θ-Ni_2Si (Fig. 6), and thus texture inheritance is possible provided that the crystal structures are related. Indeed, a minimal atomic movement is required to transform the θ-Ni_2Si into δ-Ni_2Si, as illustrated in figure 11a. The corresponding transforming planes are then: $\{010\}_\delta//\{0001\}_\theta$ for the basal plane, and $\{001\}_\delta//\{11\bar{2}0\}_\theta$ or $\{301\}_\delta//\{11\bar{2}0\}_\theta$, depending on a rotation of 60° due to the hexagonal symmetry of θ-Ni_2Si. These transformation rules well explain the change of A_θ and B_θ epitaxy into A_δ and B_δ, respectively. This is easily seen by transforming the epitaxies from Table 3 into those listed in Table 2, taking into account the symmetry of θ-Ni_2Si and the Si(001) substrate, and that an epitaxial orientation is defined by fixating the orientation of two sets of non-parallel planes. This texture inheritance not only minimises the required atomic mobility for the Si atoms, but also reduces the interface energy between the nucleated δ-Ni_2Si grain and the existing θ-Ni_2Si grain through plane-to-plane matching.

The epitaxial alignment of NiSi, which is also observed when Pt is added to the as-deposited Ni layer, can also be understood through similar epitaxial-texture inheritance arguments. Figure 11b shows that the transformation from θ-Ni_2Si to NiSi is enabled by a minimal movement of the majority of atoms involved, especially for the least-mobile element Si. The transition from compositional Ni_2Si to NiSi, however, requires the out-diffusion of half of the nickel atoms. Ellner *et al.* [37] reported that the nickel content within θ-Ni_2Si can be as low as 58 at % Ni, so this transformation is not as abrupt as displayed in figure 11b. The corresponding planes are: $\{100\}_{NiSi}//\{0001\}_\theta$ for the basal plane, and $\{013\}_{NiSi}//\{11\bar{2}0\}_\theta$ or $\{010\}_{NiSi}//\{11\bar{2}0\}_\theta$. In addition to atomic movement, this transformation requires significant deformation of the unit cells, e.g. the lattice spacing of the θ-Ni_2Si basal plane needs to expand from 4.89 to 5.18 Å. These plane transformations explain the observed transitions of A_θ to both A_{NiSi} and B_{NiSi} and B_θ into C_{NiSi}. The fact that the A_θ θ-Ni_2Si orientation results into two slightly different epitaxial phases can be related to the fact

that the texture inheritance requires some relaxation of the unit cell. It appears that the NiSi (101) and (211) planes along Si{101} orientation match with good alignment. The second orientation cannot match perfectly, due to the relaxation of the unit cell, and as such, the texture inheritance will allow small deviations around the original orientation of θ-Ni_2Si through the axiotaxial alignment.

The identified pathways for texture inheritance are depicted in Fig. 6 through arrows from the original phase to the succeeding phase. The absence of texture inheritance, for example when forming NiSi for the Ni(Al) sample, can be understood as the θ-Ni_2Si- NiSi phase sequence is interrupted by the formation of the $Ni_xAl_ySi_z$ phase. Similarly, the *in situ* XRD of Ni and Ni(Co) samples show the occurrence of non-epitaxial θ-Ni_2Si in a short temperature window just prior to the formation of NiSi. As *in situ* XRD, in the geometry used in this paper, only detects planes nearly-parallel to the surface, this observation means that the θ-Ni_2Si has lost (partially) its epitaxial alignment with the Si substrate, thus loosing the epitaxial template for epitaxial texture inheritance. Gaudet *et al.* [6] describes how θ-Ni_2Si at this temperature inherits its fiber alignment *from* fiber-aligned δ-Ni_2Si . The observation of texture inheritance of epitaxial texture (in this paper) and fiber texture (by Gaudet *et al.* [6]) in both directions between θ-Ni_2Si and δ-Ni_2Si illustrates the competitive growth of these layers.

Finally, the formation of $NiSi_2$ out of θ-Ni_2Si for the ultra-thin, 3 nm Ni films also correlates with texture inheritance (Fig. 9). The transformation rules for the formation of type-A epitaxial $NiSi_2$ out of the epitaxial A_θ θ-Ni_2Si can indeed be associated with minimal atomic movement. This is, however, less evident for the transition between B_θ and A_{NiSi_2}. It was previously suggested [10] that the low-temperature $NiSi_2$ formation in the ultra-thin regime, instead of NiSi, is the result of a much lower interface energy. Our observations corroborate this, as one epitaxial phase transforms into another, and by consequence the interface energy remains low throughout the transition both at the heterophase silicon-silicide interface, but also at the interface with the consumed silicide.

This work investigates the altered solid-phase reaction through alloying and

505 thickness reduction. The improved thermal and morphological stability of the silicide contact was already long known in literature [12, 16], and the effect of texture inheritance reported here further enhances our understanding of the underlying kinetics. A change of in preferential orientation and altered agglomeration behaviour of silicide contacts also have been reported through e.g. reducing the in-plane dimension of the contact [46, 47], removing the crystalline
510 template from the substrate through pre-amorphisation implant [48, 49, 50] or by alternating the available thermal budget during deposition [51, 52] and annealing [53, 54]. The current study therefore indicates that modern experimental techniques can further understand binary and ternary solid-phase reactions.

5. Conclusions

515 The phase formation between thin Ni films of 3 and 9 nm thickness deposited on Si(001) was investigated by means of *in situ* XRD, *in situ* sheet resistance and *ex situ* pole-figure measurements. The same measurements were also performed on samples alloyed with 10 at.% Al, Co and Pt. The measurements allowed to investigate the effect of film thickness and the presence of a ternary
520 element on the phase formation and texture of the thin nickel-silicide layers. Changes in the phase formation sequence could be interpreted on the basis of nucleation theory and the effect of entropy of mixing. Most occurring phases, i.e. the as-deposited Ni layer, δ-Ni_2Si and NiSi, revealed significant different textures upon alloying. Remarkably, θ-Ni_2Si was observed with the same epitaxial
525 orientation regardless of as-deposited thickness or alloying element, indicating the high tolerance of the θ-Ni_2Si unit cell towards impurities. The preferential orientation of subsequently-occurring silicides indicate the mechanism of texture inheritance during the phase sequence. The latter effect succeeds in explaining the occurrence of specific epitaxial and fiber textures through a transformation
530 of the preceding phases.

6. Acknowledgement

The authors acknowledge the FWO Vlaanderen, the Hercules foundation and BOF-UGent (GOA 01G01513) for providing financial support for this work. This research used resources of the National Synchrotron Light Source, a U.S. 535 Department of Energy (DOE) Office of Science User Facility operated for the DOE Office of Science by Brookhaven National Laboratory under Contract No. 405 DE-AC02-98CH10886. This research used resources of the DiffAbs beamline under guidance of C. Mocuta at the SOLEIL synchrotron, France.

References

540 [1] S. Zhang, M. Östling, Metal silicides in CMOS technology: past, present, and future trends, Critical Reviews in Solid State and Materials Sciences 28 (1) (2003) 1–129.

[2] C. Lavoie, F. d'Heurle, C. Detavernier, C. Cabral, Towards implementation of a nickel silicide process for CMOS technologies, Microelectronic 545 Engineering 70 (2) (2003) 144–157.

[3] L. Chen, Silicide technology for integrated circuits, Vol. 5, The Institution of Electrical Engineers, 2004.

[4] C. Lavoie, C. Detavernier, C. Cabral, F. dHeurle, A. Kellock, J. Jordan-Sweet, J. Harper, Effects of additive elements on the phase formation and 550 morphological stability of nickel monosilicide films, Microelectronic Engineering 83 (11) (2006) 2042–2054.

[5] D. Mangelinck, K. Hoummada, I. Blum, Kinetics of a transient silicide during the reaction of Ni thin film with (100) Si, Applied Physics Letters 95 (18) (2009) 1902.

555 [6] S. Gaudet, C. Coia, P. Desjardins, C. Lavoie, Metastable phase formation during the reaction of Ni films with Si (001): The role of texture inheritance, Journal of Applied Physics 107 (9) (2010) 093515.

[7] D. Mangelinck, K. Hoummada, F. Panciera, M. El Kousseifi, I. Blum, M. Descoins, M. Bertoglio, A. Portavoce, C. Perrin, M. Putero, Progress in the understanding of Ni silicide formation for advanced MOS structures, Physica Status Solidi (a) 211 (1) (2014) 152–165.

[8] M. El Kousseifi, K. Hoummada, M. Bertoglio, D. Mangelinck, Selection of the first Ni silicide phase by controlling the Pt incorporation in the intermixed layer, Acta Materialia 106 (2016) 193–198.

[9] K. De Keyser, C. Van Bockstael, R. Van Meirhaeghe, C. Detavernier, E. Verleysen, H. Bender, W. Vandervorst, J. Jordan-Sweet, C. Lavoie, Phase formation and thermal stability of ultrathin nickel-silicides on Si (100), Applied Physics Letters 96 (17) (2010) 173503.

[10] Z. Zhang, S. Zhang, B. Yang, Y. Zhu, S. M. Rossnagel, S. Gaudet, A. J. Kellock, J. Jordan-Sweet, C. Lavoie, Morphological stability and specific resistivity of sub-10 nm silicide films of Ni Pt_x on Si substrate, Applied Physics Letters 96 (2010) 071915.

[11] J. Luo, Z. Qiu, C. Zha, Z. Zhang, D. Wu, J. Lu, J. Åkerman, M. Östling, L. Hultman, S. Zhang, Surface-energy triggered phase formation and epitaxy in nanometer-thick $Ni_{1-x}Pt_x$ silicide films, Applied Physics Letters 96 (3).

[12] R. Tung, J. Poate, J. Bean, J. Gibson, D. Jacobson, Epitaxial silicides, Thin Solid Films 93 (1) (1982) 77–90.

[13] R. Tung, J. Gibson, J. Poate, Formation of Ultrathin Single-Crystal Silicide Films on Si: Surface and Interfacial Stabilization of Si-$NiSi_2$ Epitaxial Structures, Physical Review Letters 50 (6) (1983) 429.

[14] A. Mouroux, S.-L. Zhang, W. Kaplan, S. Nygren, M. Östling, C. Petersson, Enhanced formation of the C54 phase of $TiSi_2$ by an interposed layer of molybdenum, Applied Physics Letters 69 (7) (1996) 975–977.

585 [15] D. Mangelinck, P. Gas, J. Gay, B. Pichaud, O. Thomas, Effect of Co, Pt, and Au additions on the stability and epitaxy of $NiSi_2$ films on (111) Si, Journal of Applied Physics 84 (1998) 2583–2590.

[16] D. Mangelinck, J. Dai, J. Pan, S. Lahiri, Enhancement of thermal stability of NiSi films on (100) Si and (111) Si by Pt addition, Applied Physics 590 Letters 75 (12) (1999) 1736–1738.

[17] C. Detavernier, C. Lavoie, Influence of Pt addition on the texture of NiSi on Si (001), Applied Physics Letters 84 (18) (2004) 3549–3551.

[18] O. Cojocaru-Mirédin, D. Mangelinck, K. Hoummada, E. Cadel, D. Blavette, B. Deconihout, C. Perrin-Pellegrino, Snowplow effect and re- 595 active diffusion in the Pt doped Ni–Si system, Scripta Materialia 57 (5) (2007) 373–376.

[19] F. Panciera, D. Mangelinck, K. Hoummada, M. Texier, M. Bertoglio, A. De Luca, M. Gregoire, M. Juhel, Direct epitaxial growth of θ-Ni_2 Si by reaction of a thin Ni (10at.% Pt) film with Si (100) substrate, Scripta 600 Materialia 78 (2014) 9–12.

[20] C. Mocuta, M. Richard, J. Fouet, S. Stanescu, A. Barbier, C. Guichet, O. Thomas, S. Hustache, A. Zozulya, D. Thiaudiere, Fast pole figure acquisition using area detectors at the DiffAbs beamline–Synchrotron SOLEIL, Journal of Applied Crystallography 46 (6) (2013) 1842–1853.

605 [21] P. Pangaud, S. Basolo, N. Boudet, J.-F. Berar, B. Chantepie, P. Delpierre, B. Dinkespiler, S. Hustache, M. Menouni, C. Morel, XPAD3: A new photon counting chip for X-ray CT-scanner, Nuclear Instruments and Methods in Physics Research Section A: Accelerators, Spectrometers, Detectors and Associated Equipment 571 (1) (2007) 321–324.

610 [22] P. Pangaud, S. Basolo, N. Boudet, J.-F. Berar, B. Chantepie, J.-C. Clemens, P. Delpierre, B. Dinkespiler, K. Medjoubi, S. Hustache, et al., XPAD3-S: A fast hybrid pixel readout chip for X-ray synchrotron facilities,

Nuclear Instruments and Methods in Physics Research Section A: Accelerators, Spectrometers, Detectors and Associated Equipment 591 (1) (2008)
615 159–162.

[23] K. Medjoubi, T. Bucaille, S. Hustache, J.-F. Bérar, N. Boudet, J.-C. Clemens, P. Delpierre, B. Dinkespiler, Detective quantum efficiency, modulation transfer function and energy resolution comparison between CdTe and silicon sensors bump-bonded to XPAD3S, Journal of Synchrotron Ra-
620 diation 17 (4) (2010) 486–495.

[24] K. Medjoubi, A. Thompson, J.-F. Bérar, J.-C. Clemens, P. Delpierre, P. Da Silva, B. Dinkespiler, R. Fourme, P. Gourhant, B. Guimaraes, et al., Energy resolution of the CdTe-XPAD detector: calibration and potential for Laue diffraction measurements on protein crystals, Journal of Syn-
625 chrotron Radiation 19 (3) (2012) 323–331.

[25] K. De Keyser, C. Detavernier, Gustav: Ghent University Software for Texture Analysis and Visualisation, http://www.cocoon.ugent.be/content/gustav/.

[26] E. Verleysen, Chemical analysis of thin films in electronic devices by ana-
630 lytical transmission electron microscopy methodologies, Ph.D. thesis, KU Leuven (2013).

[27] K. De Keyser, C. Van Bockstael, C. Detavernier, R. Van Meirhaeghe, J. Jordan-Sweet, C. Lavoie, Epitaxial formation of a metastable hexagonal nickel–silicide, Electrochemical and Solid-State Letters 11 (9) (2008)
635 H266–H268.

[28] S. Gaudet, P. Desjardins, C. Lavoie, The thermally-induced reaction of thin Ni films with Si: Effect of the substrate orientation, Journal of Applied Physics 110 (11) (2011) 113524.

[29] F. Geenen, K. van Stiphout, M. Minjauw, J. Jordan-Sweet, A. Vantomme,

640 C. Lavoie, C. Detavernier, The influence of Al alloying on nickel silicide formation and texture, to be submitted.

[30] K. Richter, H. Ipser, The Al–Ni–Si phase diagram between 0 and 33.3 at.% Ni, Intermetallics 11 (2) (2003) 101–109.

[31] K. Richter, K. Chandrasekaran, H. Ipser, The Al–Ni–Si phase diagram. 645 Part II: phase equilibria between 33.3 and 66.7 at.% Ni, Intermetallics 12 (5) (2004) 545–554.

[32] K. Chandrasekaran, K. Richter, H. Ipser, The Al–Ni–Si phase diagram Part III: Phase equilibria in the nickel rich part, Intermetallics 14 (5) (2006) 491–497.

650 [33] C. Detavernier, A. Ozcan, J. Jordan-Sweet, E. Stach, J. Tersoff, F. Ross, C. Lavoie, An off-normal fibre-like texture in thin films on single-crystal substrates, Nature 426 (6967) (2003) 641–645.

[34] D. Deduytsche, C. Detavernier, R. Van Meirhaeghe, C. Lavoie, High-temperature degradation of NiSi films: Agglomeration versus $NiSi_2$ nu- 655 cleation, Journal of Applied Physics 98 (3) (2005) 033526.

[35] X. Gao, J. Andersson, T. Kubart, T. Nyberg, U. Smith, J. Lu, L. Hultman, A. J. Kellock, A. Zhang, C. Lavoie, et al., Epitaxy of ultrathin $NiSi_2$ films with predetermined thickness, Electrochemical and Solid-State Letters 14 (7) (2011) H268–H270.

660 [36] Binary Alloy Phase Diagrams, ASM international, 1996.

[37] M. Ellner, S. Heinrich, M. Bhargava, K. Schubert, Einige strukturelle untersuchungen in der mischung nisi, Journal of the Less Common Metals 66 (2) (1979) 163–173.

[38] H. Von Känel, Growth and characterization of epitaxial Ni and Co silicides, 665 Materials Science Reports 8 (5) (1992) 193–269.

[39] J. Van Beek, P. Oberndorff, A. Kodentsov, F. Van Loo, Interactions in the Co–Ni–Si system at 800 C, Journal of Alloys and Compounds 297 (1) (2000) 137–143.

[40] F. Panciera, K. Hoummada, M. Gregoire, M. Juhel, D. Mangelinck, Pt redistribution in N-MOS transistors during Ni salicide process, Microelectronic Engineering 107 (2013) 173–177.

[41] A. Schrauwen, J. Demeulemeester, D. Deduytsche, W. Devulder, C. Detavernier, C. Comrie, K. Temst, A. Vantomme, Ternary silicide formation from Ni-Pt, Ni-Pd and Pt-Pd alloys on Si (100): Nucleation and solid solubility of the monosilicides, Acta Materialia 130 (2017) 19–27.

[42] F. d'Heurle, Nucleation of a new phase from the interaction of two adjacent phases: Some silicides, Journal of Materials Research 3 (01) (1988) 167–195.

[43] M. E. Schlesinger, Thermodynamics of solid transition-metal silicides, Chemical Reviews 90 (4) (1990) 607–628.

[44] F. Geenen, W. Knaepen, F. Moens, L. Brondeel, A. Leenaers, S. Van den Berghe, C. Detavernier, Anisotropic thermal expansion of Ni, Pd and Pt germanides and silicides, Journal of Physics D: Applied Physics 49 (27) (2016) 275307.

[45] D. Smeets, A. Vantomme, K. De Keyser, C. Detavernier, C. Lavoie, The role of lattice mismatch and kinetics in texture development: $Co_{1-x}Ni_xSi_2$ thin films on Si (100), Journal of Applied Physics 103 (6) (2008) 063506.

[46] V. Svilan, K. Rodbell, L. Clevenger, C. Cabral, R. Roy, C. Lavoie, J. Jordan-Sweet, J. Harper, Dependence of crystallographic texture of C54 $TiSi_2$ on thickness and linewidth in submicron CMOS structures, in: MRS Proceedings, Vol. 427, Cambridge Univ Press, 1996, p. 53.

[47] N. Breil, C. Lavoie, A. Ozcan, F. Baumann, N. Klymko, K. Nummy, B. Sun, J. Jordan-Sweet, J. Yu, F. Zhu, et al., Challenges of nickel silicidation in CMOS technologies, Microelectronic Engineering 137 (2015) 79–87.

695 [48] Q. Liu, G. Wang, N. Duan, H. Radamson, H. Liu, C. Zhao, J. Luo, Effects of carbon pre-germanidation implantation on the thermal stability of NiGe and dopant segregation on both n-and p-type ge substrate, ECS Journal of Solid State Science and Technology 4 (5) (2015) P119–P123.

[49] S. Shenouda, G. Molnar, G. Langer, G. Katona, F. Kristaly, D. Beke,
700 Kinetics of shift of individual interfaces in Ni/Si system during low temperature reactions, Microelectronic Engineering 134 (2015) 14 – 21. doi:https://doi.org/10.1016/j.mee.2015.01.006.
URL http://www.sciencedirect.com/science/article/pii/S0167931715000155

705 [50] L. Wieluński, D. Scott, M.-A. Nicolet, H. Von Seefeld, Alteration of Ni silicide formation by N implantation, Applied Physics Letters 38 (2) (1981) 106–108.

[51] A. Sharma, S. Mohan, S. Suwas, The influence of deposition temperature on the structure, microstructure, morphology and magnetic properties of
710 sputter deposited nickel thin films, Thin Solid Films 619 (2016) 91 – 101. doi:https://doi.org/10.1016/j.tsf.2016.10.024.
URL http://www.sciencedirect.com/science/article/pii/S0040609016306125

[52] G. Dalapati, C. Tan, S. Masudy-Panah, H. Tan, D. Chi, Low temperature
715 grown highly texture aluminum alloyed iron silicide on silicon substrate for opto-electronic applications, Materials Letters 159 (2015) 455–458.

[53] M. Gregoire, R. Beneyton, P. Morin, Millisecond annealing for salicide formation: Challenges of NiSi agglomeration free process, in: Interconnect Technology Conference and 2011 Materials for Advanced Metallization
720 (IITC/MAM), 2011 IEEE International, IEEE, 2011, pp. 1–3.

[54] C. Feautrier, A. Ozcan, C. Lavoie, A. Valery, R. Beneyton, C. Borowiak, L. Clément, A. Pofelski, B. Salem, Impact of laser anneal on NiPt silicide texture and chemical composition, Journal of Applied Physics 121 (22) (2017) 225109.